doi:10.3772/j.issn.1006-6748.2019.04.009

Hopping planning of the bionic leg mechanism driven by PAMs with biarticular muscle①

Chen Ziheng (陈子衡), Lei Jingtao②, Cheng Liya, Gao Tongyue
(School of Mechatronic Engineering and Automation, Shanghai University, Shanghai 200072, P. R. China)

Abstract

Bionic robots are generally driven by motors. As robots driven by pneumatic artificial muscles (PAMs) have the advantages of light weight, good bionics and flexibility, more and more researchers have adopted PAMs to drive bionic robots. A kind of bionic leg driven by PAMs for hopping is proposed in this work. A 3-DOF bionic leg driven by 4 PAMs is designed by analyzing the biological structure and movement principles of frog legs, and 3 kinds of leg configuration with different PAMs arrangement is proposed. One biarticular muscle is used to increase the joint rotating range. The bracket pulley and PAMs for driving joint can effectively increase its rotating range. The rotating range of hip and knee joint driven by a biarticular muscle is simulated. The simulation results show that the biarticular muscle can transfer the movement of the hip joint to the knee joint and increase the rotating range of the knee joint. The greater the contraction of PAM, the greater the rotating range of joint. The bionic leg can perform planned step distance and step height of hopping.

Key words: bionic leg, pneumatic artificial muscle (PAM), biarticular muscle, bionic hopping, trajectory planning

0 Introduction

Compared with wheeled or tracked robots, the leg-type hopping robot has greater flexibility, obstacle avoidance capability and autonomy. With the development of bionic technology, hopping robots such as humanoid robot, bionic kangaroo, bionic scorpion and bionic frog, have emerged[1]. Deng et al[2] studied the take-off principles and hopping planning as well as the optimization of a hopping robot, parameterized the joint space trajectory by adopting the Fourier primary function, and optimized the take-off performance. For the underactuated constraint formed between the sole and the ground during the hopping process of frog-like hopping robot and the specific hopping task, Hu et al[3] proposed a path planning control to achieve the given take-off task in the task space to improve system performance. Partial feedback linearization is used to linearize the nonlinear part of the take-off dynamics of the frog-like hopping robot, design sliding mode variable structure controller, track and control the centroid trajectory of the frog-like hopping robot. Wang et al[4] simplified the single-legged jumping robot to a 3-bar model, studied the motion trajectory of each joint during the robot hopping, and used a parametric optimization method to realize trajectory planning in the joint space. Gao et al[5] established a single-legged kinematics model of a hydraulically driven 4-legged robot, determined the driving function by the inverse kinematics, and used the virtual prototype technology to simulate the vertical jumping gait and verify the accuracy and rationality of the gait planning. Wang et al[6] established a frog-like hopping robot, analyzed the joint trajectory of the hind limb during its jumping movement, the important influence of the foot and the supporting role of the forelimb on the body by the biological observation and kinematic. Chen et al[7] proposed a rigid-flexible coupling hopping mechanism inspired by locusts' hopping and analyzed its kinematics. The results show that the proposed bionic mechanism has good kinematics performance and can provide a basis for robot design and motion planning. Chen[8] analyzed the kinematics of the jumping process of locusts by using a high-speed photography to obtain jumping parameters of locusts, used the virtual prototype technology to build a locust-like model to analyze the displacement, velocity, acceleration and force of locust during the jump process. Chen[9] analyzed the movement posture and joint size of the leg of the athletes during jump

① Supported by the National Natural Science Foundation of China (No. 51775323, 51375289).
② To whom correspondence should be addressed. E-mail: jtlei2000@163.com
Received on Aug. 18, 2018

by high-speed camera, built a simplified model of hopping robot, and analyzed changing of the angular displacement of the hip, knee and ankle joints, which lay a theoretical foundation for developing the humanoid hopping robot. Niiyama et al[10] developed Mowgli which was a 2-legged robot driven by 6 pneumatic artificial muscles (PAMs), including biarticular PAMs. The experiments showed that Mowgli could jump up to 1.5 times its height and could land smoothly. Narioka et al[11] developed Ken which was a small 4-legged robot driven by PAMs. It provided power for high frequency and wide stride movements. Hosoda et al[12] imitated the structure and role of the human leg to design a biped hopping robot driven by PAMs through analyzing the human leg skeleton. The biped hopping robot was driven by 9 PAMs, three of which were biarticular muscles. The experiments showed that when the knee or the hip was stretched out, the biarticular muscles could effectively coordinate the movements of the joints. The extension of the ankle joint does not produce coordinated movements. The results can be used not only for robotics, but also for studying on the adaptive human mechanisms. Yamada et al[13] developed a quadruped musculoskeletal robot with biological realistic morphology and a nervous system, which deepens a comprehensive understanding of how the body and nervous system jointly produce animal movements. Nishikawa et al[14] proposed a bionic quadruped robot driven by PAMs. The robot was designed with an angle-dependent moment arm (ADMA) with biased pivot, which could expand the range of postures effectively that robots could take during dynamic motions. Zhang et al[15] established 3 different leg mechanism models based on the physiological structure and research status of the locust legs, performed kinematics and dynamics analysis of the legs. The performance index of maximum buffer distance, energy absorption capacity and mechanical properties were obtained. Nishikawa et al[16] proposed a torque-angle relationship control system (TARCS) for musculoskeletal robots, tested its static properties, and used TARCS to improve the performance of the robot. They studied the hopping ability by simulation. It was found that the TARCS in a biarticular muscle determined the general shape of the jumpable range. Waycaster et al[17] developed an above-knee prosthesis driven by PAMs, and demonstrated the PAM actuation's capability in generating sufficient torque output to meet the locomotion needs. A model torque control algorithm based on the synovial control method was designed to restore the motion function. Ryuma et al[18] developed a kind of musculoskeletal robot for biomechanical research. The robot could hop vertically and the hop height could reach 1 m. Sato et al[19] found biarticular muscles could play an important role. A bionic leg driven by a biarticular muscle was developed. The experimental results showed that the biarticular muscle could improve the performance of hopping and landing of the leg effectively. Kazama et al[20] developed a bionic leg driven by a spring and a biarticular muscle to improve the dynamic movement performance of the robot like a creature. They found the hind legs driven by a biarticular muscle played an important role in hopping.

The bionic leg driven by PAMs is studied in this work. Three different leg configurations with different PAM arrangements are proposed. The kinematics of the bionic hopping is analyzed. The geometric method is adopted to analyze the leg with 3 PAM arrangements. The optimal configuration of leg is determined according to the joint rotating range. The centroid trajectory is calculated according to the hopping planning of the bionic leg with a variable quintic polynomial. It is shown that the joint angle obtained according to the PAM arrangement can achieve the planned step distance and step of hopping.

1 Bionic hopping kinematics

According to the constraint relationship between foot and ground, a hopping process of the bionic legs can be divided into take-off phase, flight phase and landing phase, as shown in Fig. 1.

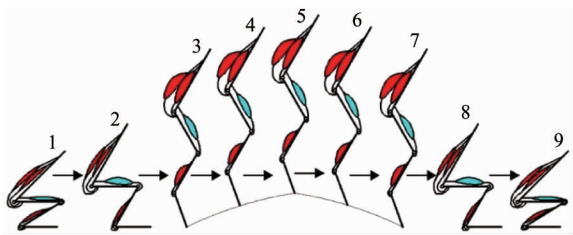

1 the leg in the initial state; 2 the stretching posture of the leg under the action of biarticular muscles; 3 the leg in the state of the toe will leave the ground; 4, 5 and 6 the leg in the flight phase; 7 the leg tiptoe touches the ground; 8 the leg in landing state; 9 the bionic leg returns to the initial state.

Fig. 1 Hopping processes

1.1 Bionic leg configuration and PAM arrangement

The bionic leg configuration is shown in Fig. 2(a). There are 2 types of PAMs. One is the Mckibben PAM from Japan, the other is the Festo PAM from Germany. Considering the mechanical configuration of the bionic leg, joint size, contraction rate and PAM installation, the DMSP-PAM from Festo company is selected in this paper, as shown in Fig. 2(b). It has a shrinkage of

25%. Compared with MAS-PAM from Festo company, the DMSP-PAM does not require extra accessories and can be connected. PAMs are lighter in weight and has the advantages of small interface size. Under the same muscle length conditions, there is a relatively large amount of contraction.

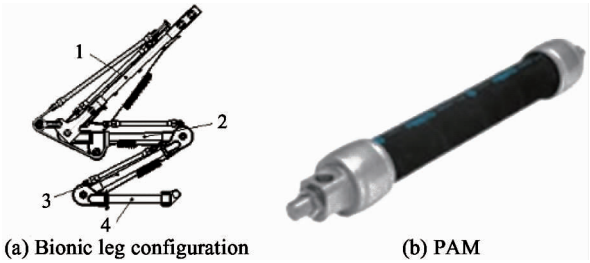

1 the body; 2 the thigh skeleton; 3 the calf skeleton; 4 the foot end skeleton

Fig. 2 Bionic leg configuration and PAM

According to the bionic leg configuration, three different PAM arrangements are proposed, as shown in Fig. 3. In Fig. 3(a), monoarticular muscle *Gmax-B* is used to drive the hip joint; biarticular muscle *K-BM* is used to drive the hip and knee joints; finally monoarticular muscle *AM* is used to drive the ankle joint. In Fig. 3(b), 2 monoarticular muscles *Gmax-A* and *Gmax-B* are used to drive the hip joint; biarticular muscle *K-BM* is used to drive the hip and knee joints; the single joint muscle *AM* is used to drive the ankle joint. In Fig. 3(c), 2 monoarticular joint muscles *Gmax-A* and *Gmax-B* are used to drive the hip joint; monoarticular joint muscle *K-BM* is used to drive the knee joints; monoarticular muscle *AM* is used to drive the ankle joint.

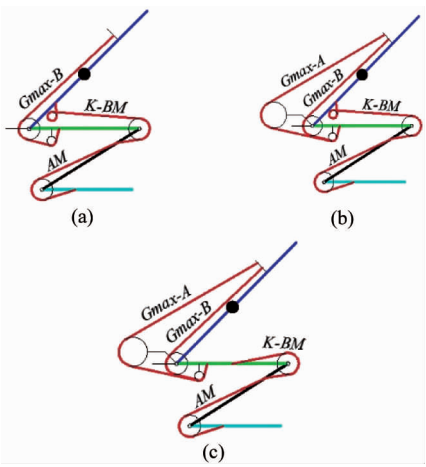

Fig. 3 Leg configuration with different PAMs arrangement

1.2 Kinematics of leg during take-off stage

Assuming that there is no relative sliding between the foot and the ground, the foot end is equivalent to a passive joint due to the presence of a passive ankle. D-H coordinate method is used to analyze the kinematics of bionic hopping. Homogeneous transformation matrix is used to describe the pose relationship between adjacent links. The D-H coordinate system of each link is established on the simplified model of the bionic leg. As shown in Fig. 4, where θ_1, θ_2, θ_3 and θ_4 are foot joint variables, ankle joint variables, knee joint variables, and hip joint variables respectively. l_1, l_2, l_3 and l_4 are body length, thigh skeleton length, leg skeleton length and foot end length respectively.

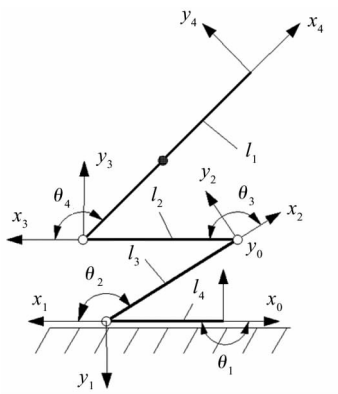

Fig. 4 D-H coordinate systems of leg during take-off stage

The general transformation formula using the post-coordinate system ${}^{i-1}_{i}\boldsymbol{T}$ is

$$ {}^{i-1}_{i}\boldsymbol{T} = \begin{bmatrix} c\theta_i & -s\theta_i c\alpha_i & s\theta_i s\alpha_i & \alpha_i c\theta_i \\ s\theta_i & c\theta_i c\alpha_i & -c\theta_i s\alpha_i & \alpha_i s\theta_i \\ 0 & s\alpha_i & c\alpha_i & d_i \\ 0 & 0 & 0 & 1 \end{bmatrix} \tag{1} $$

where $i = 1,2,3,4$, $\theta_i = \pi$, $c\theta_i = \cos\theta_i$, $s\theta_i = \sin\theta_i$, $\alpha_i = 0$, $c\alpha_i = \cos\alpha_i$, $s\alpha_i = \sin\alpha_i$.

1.2.1 Positive kinematics

Positive kinematics of leg is that the variables of each joint is known to solve the position and pose of D-H coordinate system. The transformation matrix ${}^{0}_{4}\boldsymbol{T}$ of D-H coordinate system relative to the base coordinate system is obtained by multiplying each link transformation matrix:

$$ {}^{0}_{4}\boldsymbol{T} = {}^{0}_{1}\boldsymbol{T} \cdot {}^{1}_{2}\boldsymbol{T} \cdot {}^{2}_{3}\boldsymbol{T} \cdot {}^{3}_{4}\boldsymbol{T} = \begin{bmatrix} n_x & o_x & a_x & p_x \\ n_y & o_y & a_y & p_y \\ n_z & o_z & a_z & p_z \\ 0 & 0 & 0 & 1 \end{bmatrix} \tag{2} $$

It is a function of θ_1, θ_2, θ_3 and θ_4.

1.2.2 Inverse kinematics

Inverse kinematics used matrix ${}^{0}_{4}\boldsymbol{T}$ of the body coordinate system relative to the base coordinate system to solve joint variables θ_1, θ_2, θ_3 and θ_4.

Given:

$$
{}^{0}_{4}\boldsymbol{T} = \begin{bmatrix} n_x & o_x & a_x & p_x \\ n_y & o_y & a_y & p_y \\ n_z & o_z & a_z & p_z \\ 0 & 0 & 0 & 1 \end{bmatrix} = {}^{0}_{1}\boldsymbol{T}(\theta_1) \cdot {}^{1}_{2}\boldsymbol{T}(\theta_2) \cdot {}^{2}_{3}\boldsymbol{T}(\theta_3) \cdot {}^{3}_{4}\boldsymbol{T}(\theta_4) \quad (3)
$$

The inverse kinematics of the leg during take-off stage by inverse transformation method is

$$
\begin{cases} \theta_2 = 2\arctan \dfrac{A - \sqrt{A^2 + B^2 - C^2}}{B + C} \\ \theta_3 = \arctan \dfrac{p_y(c_2 n_x + s_2 n_y) + p_x(s_2 n_x - c_2 n_y) + l_2 s_2}{-p_x(c_2 n_x + s_2 n_y) + p_y(s_2 n_x - c_2 n_y) - l_3 - l_2 c_2} \\ \theta_4 = \arctan \dfrac{l_4 s_{23} + p_x s_{23} - p_y c_{23} + s_3 l_3}{-l_2 - l_4 c_{23} - p_x c_{23} - p_y s_{23} - c_3 l_3} \end{cases} \quad (4)
$$

where A, B, C are

$$
A = -2l_3(l_1 n_y + p_y)
$$

$$
B = 2l_3(l_1 n_x + l_3 + p_x)
$$

$$
C = l_2^2 - l_3^2 - (l_1 n_y + p_y)^2 - (l_1 n_x + l_4 + p_x)^2
$$

where $c_2 = \cos\theta_2$, $s_2 = \sin\theta_2$, $c_{23} = \cos(\theta_2 + \theta_3)$, $s_{23} = \sin(\theta_2 + \theta_3)$.

2 Joint angle and PAM length

For the proposed 3 configurations of the bionic leg as shown in Fig. 3, the relationship between PAM length and joint angle is analyzed by the geometrical method. Different driving systems of the hip joint muscle system, hip and knee joint muscle system and ankle muscle system are analyzed respectively.

2.1 Muscular system of hip joint

For the hip joint muscle system, comparison is carried out by simulation for muscle layout in Fig. 3(a) and muscle layout in Fig. 3(b). For muscle arrangement in Fig. 3(a), only PAM *Gmax-B* is inflated. For situation in Fig. 3(b), the PAM *Gmax-A* is inflated after the contraction of the PAM *Gmax-B* reaches the maximum.

The non-pulley support muscle system of the hip joint in Fig. 3(a) is shown in Fig. 5.

The length of muscle *Gmax-B* is set as l_B, then

$$
l_B = x_5 + x_6 + x_7 + x_8 \quad (9)
$$

The distance between 2 pulleys is calculated:

$$
l_1 = \sqrt{c^2 + d^2} \quad (10)
$$

thus:

$$
x_7 = \sqrt{l_1^2 - (r - r_2)^2} \quad (11)
$$

According to the geometric relationship, x_5 can be calculated as

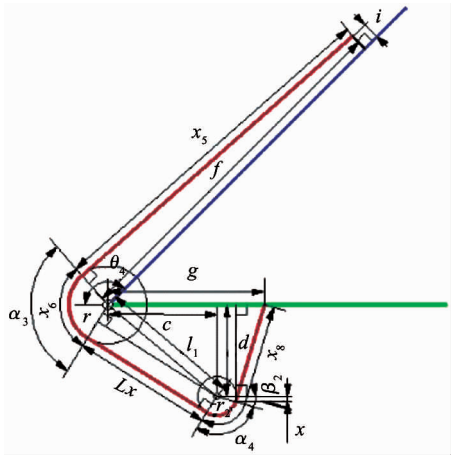

Fig. 5 PAM *Gmax-B* connection of the hip joint

$$
x_5 = \sqrt{f^2 + i^2 - r^2} \quad (12)
$$

From the angle α_3 in Fig. 5, x_6 can be calculated as

$$
x_6 = r\alpha_3 \quad (13)
$$

where

$$
\alpha_3 = \pi + \theta_4 - \arctan\frac{i}{f} - \arctan\frac{x_5}{r} - \arctan\frac{d}{c} - \arctan\frac{x_7}{r - r_2}
$$

From the geometric installation size, x is

$$
x = \frac{-2dr_2^2 + \sqrt{4d^2r_2^4 + 4r_2^2(c^2 + d^2 - 2cg + g^2)(c^2 + g^2 - 2cg - r_2^2)}}{2(c^2 + d^2 - 2cg + g^2)}
$$

therefore:

$$
\begin{cases} \beta_2 = \arcsin\dfrac{x}{r_2} \\ \alpha_4 = \pi - \beta_2 - \arctan\dfrac{r - r_2}{x_7} - \arctan\dfrac{c}{d} \end{cases}
$$

It can be obtained from the geometric relationship that:

$$
x_8 = r_2\alpha_4 + \frac{r_2(g - c - \sqrt{r_2 - x^2})}{x} \quad (14)
$$

For the leg configuration shown in Fig. 3(a), the pulley and PAMs of hip joint is shown in Fig. 6. Given the length of the PAM *Gmax-A* is l_A, according to the geometric relationship, then

$$
l_A = x_1 + x_2 + x_3 + x_4 \quad (15)
$$

The distance between the 2 pulleys is

$$
l = \sqrt{x_a^2 + y_a^2}
$$

where

$$
\begin{cases} x_a = a + b\sin\theta_4 + c \\ y_a = d - b\cos\theta_4 \end{cases}
$$

x_3 is obtained:

$$
x_3 = \sqrt{l_2 - (r_1 - r_2)^2} \quad (16)
$$

For the solution of x_1 and x_2:

$$\begin{cases} x_1 = \sqrt{x_b^2 + y_b^2 - r_1^2} \\ x_2 = r_1\beta_1 \end{cases} \tag{17}$$

where

$$\begin{cases} x_b = a + b\sin\theta_4 - f\cos\theta_4 - h\sin\theta_4 \\ y_b = f\sin\theta_4 + b\cos\theta_4 - h\cos\theta_4 \\ \Phi_1 = \arccos\dfrac{r_1 - r_2}{l} \\ \beta_1 = 2\pi - \Phi_1 - \arctan\dfrac{y_b}{x_b} - \arctan\dfrac{y_a}{x_a} - \arctan\dfrac{x_1}{r_1} \end{cases}$$

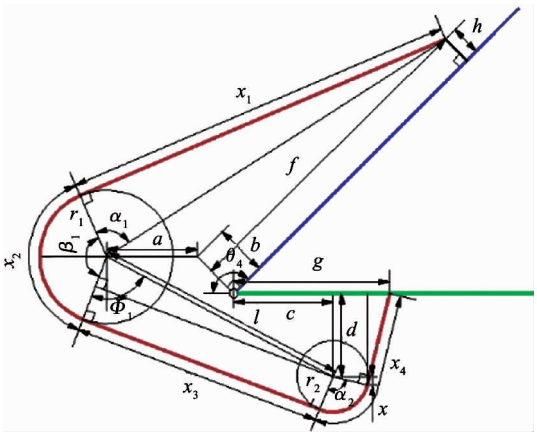

Fig. 6 PAM *Gmax-A* connection of hip joint

The value of x and α_2 obtained by the geometric method is

$$\begin{cases} x = \dfrac{-2dr_2^2 + \sqrt{4d^2r_2^4 + 4r_2^2(c^2 + d^2 - 2cg + g^2)(c^2 + g^2 - 2cg - r_2^2)}}{2(c^2 + d^2 - 2cg + g^2)} \\ \alpha_2 = \pi - \arctan\dfrac{r_1 - r_2}{l} - \arctan\dfrac{x_b}{y_b} - \arctan\dfrac{x}{r_2} \end{cases}$$

then

$$x_4 = r_2\alpha_2 + \frac{r_2(d + x)}{g - c - \sqrt{r_2^2 - x^2}} \tag{18}$$

2.2 Muscular system of hip joint and knee joint

For hip and knee muscle arrangement, two cases of Fig. 3(b) and Fig. 3(c) are analyzed and compared. One is to use a monoarticular muscle to drive the knee joint, the other is to use a biarticular muscle to drive the hip and knee joints.

For the muscle arrangement shown in Fig. 3(b), the biarticular muscle system of the hip and knee joints is shown in Fig. 7. The length of the muscle *K-BM* is l_{BM},

$$l_{BM} = x_9 + x_{10} + x_{11} \tag{19}$$

From the cosine theorem of the triangle function, the distance between the 2 pulleys is

$$l_2 = \sqrt{j^2 + n^2 + m^2 - 2Am\cos\Phi_2}$$

then

$$x_{10} = \sqrt{l_2^2 - (r - r_3)^2} \tag{20}$$

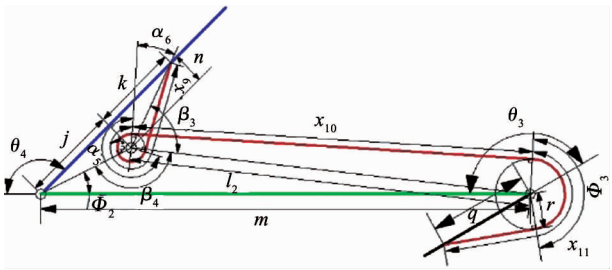

Fig. 7 Biarticular muscle connection of knee joint

Through geometric calculation, x_9 and x_{11} are

$$\begin{cases} x_9 = \sqrt{k^2 + n^2 - r_3^2} + r_3\alpha_5 \\ x_{11} = \sqrt{q^2 + r^2} + r\Phi_3 \end{cases} \tag{21}$$

where the angles are

$$\begin{cases} \alpha_5 = 2\pi - \alpha_6 - \arctan\dfrac{k^2 + n^2 - r_3^2}{r_3} \\ \alpha_6 = \dfrac{\pi}{2} - \beta_3 + \arctan\dfrac{r - r_3}{x_{10}} \\ \beta_3 = 2\pi - \arctan\dfrac{k}{n} - \arctan\dfrac{j}{n} - \beta_4 \\ \beta_4 = \arccos\dfrac{j^2 + n^2 + l_2^2 - m^2}{2l_2\sqrt{j^2 + n^2}} \\ \Phi_2 = \pi - \theta_4 - \arctan\dfrac{n}{j} \\ \Phi_3 = \pi + \theta_3 - \arctan\dfrac{r}{q} - \arccos\dfrac{l_2^2 + m^2 - j^2 - n^2}{2l_2m} \end{cases}$$

For the muscle arrangement shown in Fig. 3(c), the monoarticular muscle system of the knee joint is shown in Fig. 8.

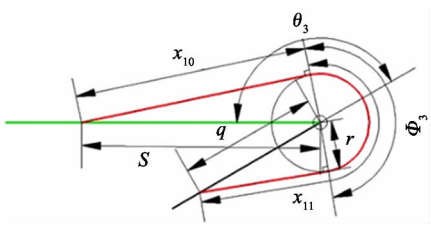

Fig. 8 Monoarticular muscle connection of knee joint

Given the length of the muscle *K-BM* is l_{BM}, then

$$l_{BM} = x_{10} + x_{11} \tag{22}$$

From the geometric relationship, x_{10} and x_{11} are

$$\begin{cases} x_{10} = \sqrt{s^2 + r^2} \\ x_{11} = r\Phi_3 + \sqrt{q^2 - r^2} \end{cases} \tag{23}$$

where

$$\Phi_3 = \pi + \theta_3 - \arccos\frac{r}{s} - \arccos\frac{r}{q}$$

2.3 Muscular system of ankle joint

The ankle joint muscle system is shown in Fig. 9.

Given the length of muscle AM is l_{AM}, the following can be obtained from the geometric relationship.

$$l_{AM} = \sqrt{p^2 - r^2} + r\Phi_5 + \sqrt{z^2 - r^2} \tag{24}$$

where

$$\Phi_5 = \pi + \theta_2 - \arccos\frac{p}{r} - \arccos\frac{z}{r}$$

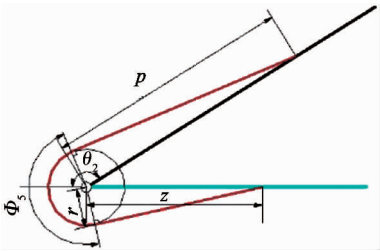

Fig. 9 PAM connection of the ankle joint

3 Centroid trajectory planning

Analyzing the centroid trajectory of bionic leg hopping is one of the main contents of hopping motion planning. To ensure that the bionic leg centroids have a certain initial velocity at the moment of leaving the ground and that the bionic leg can hop smoothly and cross an obstacle of a certain height, it is necessary to plan the centroid motion of the bionic leg. Variable quintic polynomial is used to compare the centroid motion of the bionic leg. The variable quintic polynomial is tunable parameters with added additional items based on quintic polynomial, so that the variable quintic polynomial cannot satisfy the motion constraint condition only, but also adjust the shape of the curve. The centroid trajectory of leg during the take-off stage is planned as

$$\begin{cases} x_1(t) = \sum_{i=0}^{5} a_i t^i + u_1 (t - t_s)^{\lambda_1} (t - t_f)^{\lambda_2} \\ y_1(t) = \sum_{i=0}^{5} b_i t^i + u_2 (t - t_s)^{\lambda_3} (t - t_f)^{\lambda_4} \end{cases} \tag{25}$$

where $x_1(t)$, $y_1(t)$ are the coordinates of the bionic leg centroid in the x-direction and y-direction of the foot-end coordinate system at the time of t. a_i and b_i are polynomial coefficients. u_1, u_2, $\lambda_i (i = 1,2,3,4, \lambda_i \geqslant 3)$ are curve tunable parameters. t_s and t_f are the initial and end time of the jump phase respectively.

At the initial time of the take-off stage, the motion constraint condition of the bionic leg centroid is

$$\begin{cases} x_1^{ts} = x_1,\ y_1^{ts} = y_1 \\ v_x^{ts} = 0,\ v_y^{ts} = 0 \\ a_x^{ts} = 0,\ a_y^{ts} = 0 \end{cases} \tag{26}$$

where x_1, y_1 are the center-of-mass coordinate of the bionic leg in the initial phase of the take-off phase. These 2 parameters are determined according to the specific configuration of the bionic leg. As the bionic leg is in stationary state at the initial time of the take-off stage, the speed and acceleration of the bionic leg centroid are zero.

At the end time of the take-off stage, the motion constraints of the bionic leg centroid are

$$\begin{cases} x_1^{tf} = x_2,\ y_1^{tf} = y_2 \\ v_x^{tf} = v_{2x},\ v_y^{tf} = v_{2y} \\ a_x^{tf} = 0,\ a_y^{tf} = -g \end{cases} \tag{27}$$

where x_2 and y_2 are the center-of-mass coordinates of the bionic leg at the end time of the take-off phase. These 2 parameters are determined by the stretching of the bionic leg at the end of the take-off phase. v_{2x} and v_{2y} are the velocities of the bionic leg centroids in the x and y directions of the foot coordinate system at the end of the take-off stage. These 2 parameters are height h of the obstacle and horizontal distance s from the foot end of the bionic leg to the obstacle, as shown in Fig. 10. As the movement of bionic legs after the flight can be regarded as the oblique projectile motion of the bionic leg, then v_{2x} and v_{2y} are

$$\begin{cases} v_{2x} = \dfrac{s}{\sqrt{\dfrac{2h}{g}}} \\ v_{2y} = \sqrt{2gh} \end{cases} \tag{28}$$

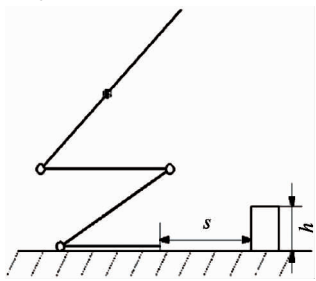

Fig. 10 Step distance and height of leg hopping

4 Simulation

The simulation analysis on the hopping of the bionic leg driven by PAM is carried out to determine the centroid trajectory simulation fitting planning at the take-off stage. The hopping step parameters are set as step distance $s = 100$ mm, and step height $h = 100$ mm. The initial value of joint angles are set as $\theta_4 = -2\pi/3$, $\theta_3 = 5\pi/12$, $\theta_2 = -3\pi/4$.

4.1 Simulation of muscular system

Based on the relationship between the changes in muscle length and the joint angle given by Eqs(9), (15), (19), (22) and (24), the joint angles of the bionic leg can be obtained by inverse solution. For 3

different PAM arrangements, the change of joint angle obtained by Matlab/Simulation according to the contraction of the pneumatic muscle is shown in Fig. 11 – Fig. 13.

It can be seen from Fig. 11(a) that the variation range of θ_4 is 60.3113°. According to the initial value of θ_4, its rotating range is from −120° to −59.6887°, which is the rotating range of the hip joint with muscle arrangement shown in Fig. 3(a).

It can be seen from Fig. 11(b) that the variation range of θ_4 is 17.9181°, and then combined with the rotating range of joint angle θ_4 caused by PAM *Gmax-B*, the final rotating range is from −120° to −41.7706°, which is the rotating range of the hip joint with the muscle arrangement shown in Fig. 3(b).

Comparing and analyzing the data in Fig. 11(a) and (b), it can be found that the rotating range of the hip angle is enlarged by adding a pulley system.

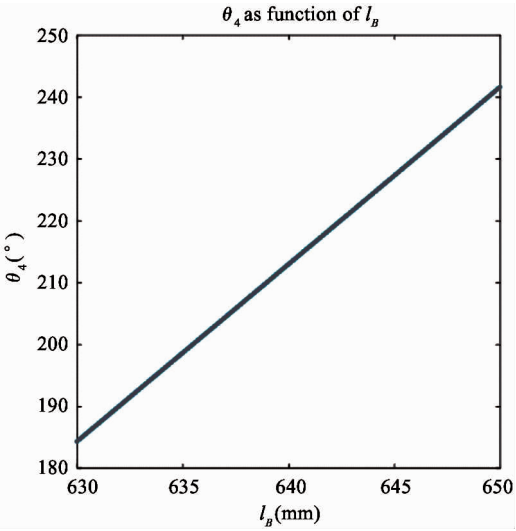

(a) Variation range of joint angle θ_4 driven by PAM *Gmax-B*

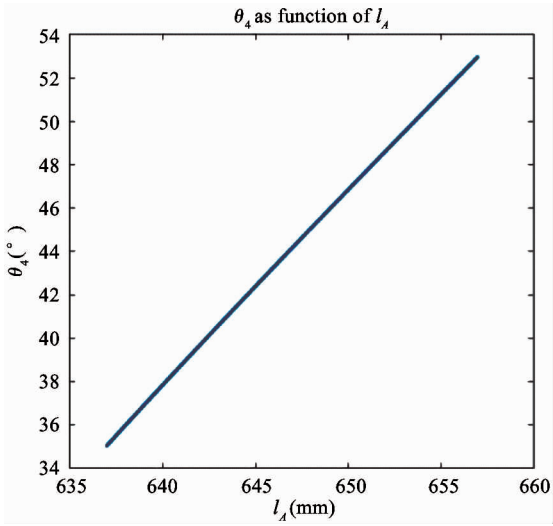

(b) Variation range of joint angle θ_4 driven by PAM *Gmax-A*

Fig. 11 Relationship between hip joint angle and PAM length

It can be seen from Fig. 12(a) that the variation range of θ_3 is 57.2958°. According to the initial value of θ_3, its rotating range is from 75° to 132.2958°, which is the rotating range of the knee joint with the muscle arrangement shown in Fig. 3(b).

It can be seen from Fig. 12(b) that the variation range of θ_3 is 49.8224°. According to the initial value of θ_3, its rotating range is from 75° to 124.8224°,

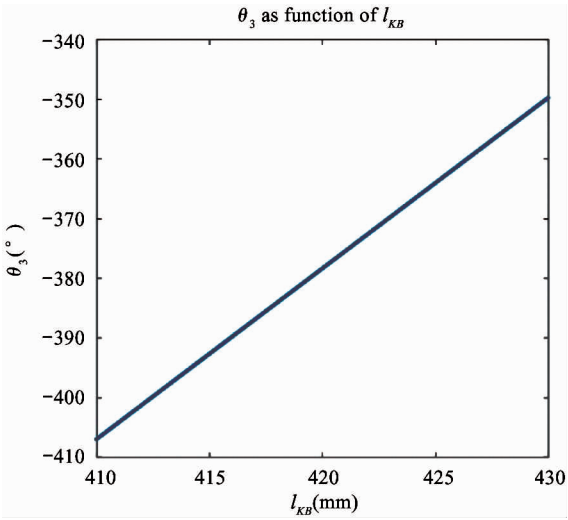

(a) Variation range of knee joint angle θ_3 driven by a biarticular muscle *K-BM*

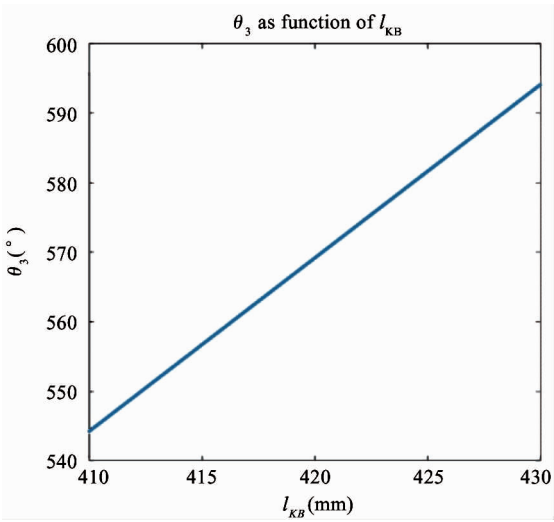

(b) Variation range of knee joint angle θ_3 driven by a monoarticular muscles *K-BM*

Fig. 12 Relationship between knee joint angle and PAM length

which is the rotating range of the knee joint with the muscle arrangement shown in Fig. 3(c).

Comparing and analyzing the data in Fig. 12(a) and Fig. 12(b), it can be found that greater rotating angle of knee joint can be obtained using a biarticular muscle. At the same time, it is found that the more the PAM contracts, the greater the rotating range of joint.

It can be seen from Fig. 13 that the variation range of θ_2 is 45.8366°. According to the initial value of θ_2, its rotating range is from −135° to −89.1634°.

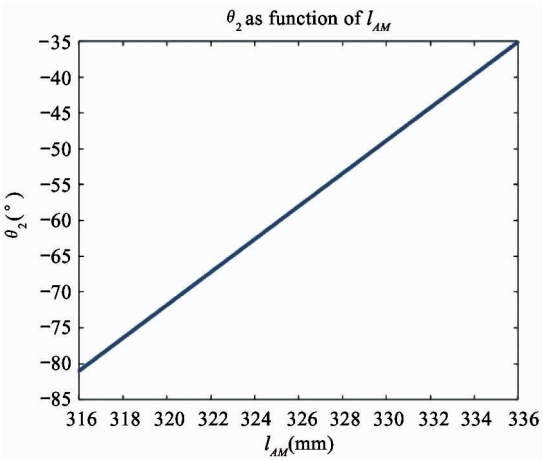

Fig. 13 Relationship between ankle joint angle and muscle *AM* length

4.2 Centroid workspace and trajectory

For the bionic leg shown in Fig. 3(b), the workspace and trajectory of the bionic leg centroid are analyzed.

$$\begin{bmatrix} x \\ y \\ z \\ 1 \end{bmatrix} = {}^{0}_{4}\boldsymbol{T} \cdot \begin{bmatrix} x_0 \\ y_0 \\ z_0 \\ 1 \end{bmatrix} \tag{29}$$

where ${}^{0}_{4}\boldsymbol{T}$ is the transformation matrix of the positive kinematics of bionic leg. x_0, y_0 and z_0 are the initial coordinates of the centroid, respectively. x, y and z are the instantaneous coordinates of the centroid, respectively.

The centroid workspace of the bionic leg in the foot-end coordinate system can be calculated by Eq. (29), as shown in Fig. 14. According to the initial values of the centroid coordinates, the centroid trajectory can be calculated by Eq. (25), as shown in Fig. 14.

It can be seen that proposed hopping planning with given hopping parameters can ensure the centroid trajectory location within its workspace.

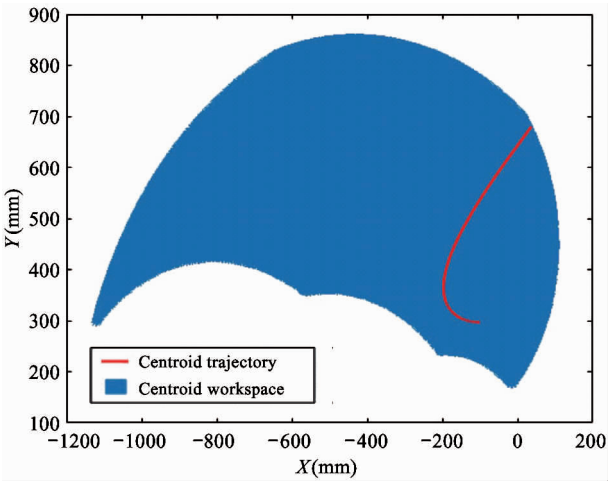

Fig. 14 Centroid trajectory and workspace

5 Conclusions

The hopping planning of the bionic leg driven by PAMs is studied. Firstly, according to the configuration and geometric relationship of the bionic leg, the relationship between the PAM length and the joint angles of the bionic leg is analyzed. The joint rotating range is compared with three different PAM arrangements. It is found that the pulley and PAM system can extend the rotating range of the hip joint. Secondly, by analyzing the range of hip and knee joint driven by a biarticular muscle, it is found that the biarticular muscle can transmit the movement of the hip joint angle to the knee joint angle and increase the rotating range of the knee joint. The greater the PAM contracts, the larger the joint rotating range. Finally, the centroid trajectory of the bionic leg is planned as a variable quantic polynomial during the take-off stage of bionic leg, which can be completely located within the centroid workspace formed by changing the joint angles, which shows that the proposed bionic leg with PAM arrangement can achieve the planned hopping motion.

Reference

[1] Wei D W, Ge W J. Research status and trends of jumping robots[J]. *Robot*, 2014, 36(4):503-512

[2] Deng K, Guo B, Xu P, et al. Analysis of motion planning and take-off mechanism for a multi-joint jumping robot[J]. *Applied Science and Technology*, 2012, 39(4): 25-30

[3] Hu S H, Deng K X, Guo B, et al. Take-off task planning and control for bionic frog jumping robot[J]. *Computer Simulation*, 2013, 30(7):341-344

[4] Wang S J, Guo Z H. Trajectory planning of one-legged-hopper robot[J]. *China Mechanical Engineering*, 2015, 26(17): 2330-2335

[5] Gao B W, Wang S K, Gao Y F. Single leg vertical hopping gait planning for hydraulic quadruped robot[J]. *Chinese Journal of Scientific Instrument*, 2017, 38(5): 1086-1092

[6] Wang M, Zang X Z, Fan J Z, et al. Biological jumping mechanism analysis and modeling for frog robot[J]. *Journal of Bionic Engineering*, 2008, 5(3):181-188

[7] Chen D C, Yin J M, Zhao K, et al. Bionic mechanism and kinematics analysis of hopping robot inspired by locust jumping[J]. *Journal of Bionic Engineering*, 2011, 8(4):429-439

[8] Chen Y. Jumping mechanism and simulation of the locust-like robot[C]//Proceedings of the 2010 2nd International Conference on Education Technology and Computer, Shanghai, China, 2010: 68-72

[9] Chen Y. Biological jumping characteristic of the humanoid robot[C]//Proceedings of the 2010 International Conference on Computer, Mechatronics, Control and Electronic Engineering, Changchun, China, 2010: 29-12

[10] Niiyama R, Nagakubo A, Kuniyoshi Y. Mowgli: a bipedal jumping and landing robot with an artificial musculoskeletal system[C]//Proceedings of the 2007 IEEE International Conference on Robotics and Automation, Roma, Italy, 2007: 2546-2551

[11] Narioka K, Rosendo A, Sproewitz A, et al. Development of a minimalistic pneumatic quadruped robot for fast locomotion[C]//Proceedings of the 2012 IEEE International Conference on Robotics and Biomimetics (ROBIO), Guangzhou, China, 2012: 307-311

[12] Hosoda K, Sakaguchi Y, Takayama H, et al. Pneumatic-driven jumping robot with anthropomorphic muscular skeleton structure[J]. *Autonomous Robots*, 2010, 28(3): 307-316

[13] Yamada Y, Nishikawa S, Shida K, et al. Neural-body coupling for emergent locomotion: a musculoskeletal quadruped robot with spinobulbar model[C]//Proceedings of the 2011 IEEE/RSJ International Conference on Intelligent Robots and Systems, San Francisco, USA, 2011: 1499-1506

[14] Nishikawa S, Tanaka K, Shida K, et al. A musculoskeletal bipedal robot designed with angle-dependent moment arm for dynamic motion from multiple states[J]. *Advanced Robotics*, 2014, 28(7):487-496

[15] Zhang Z Q, Chen D S, Chen K W. Analysis and comparison of three leg models for bionic locust robot based on landing buffering performance[J]. *Science China Technological Sciences*, 2016, 59: 1413-1427

[16] Nishikawa S, Shida K, Kuniyoshi Y. Musculoskeletal quadruped robot with torque-angle relationship control system[C]//Proceedings of the 2016 IEEE International Conference on Robotics and Automation (ICRA), Stockholm, Sweden, 2016: 4044-4050

[17] Waycaster G, Wu S K, Shen X. Design and control of a pneumatic artificial muscle actuated above-knee prosthesis [J]. *Journal of Medical Devices*, 2011, 5(3):031003

[18] Ryuma N, Yasuo K. Pneumatic biped with an artificial musculoskeletal system[C]//Proceedings of the 4th International Symposium on Adaptive Motion of Animals and Machines, Cleveland, USA, 2008: 80-81

[19] Sato R, Miyamoto I, Sato K, et al. Development of robot legs inspired by bi-articular muscle-tendon complex of cats[C]//Proceedings of the 2015 IEEE/RSJ International Conference on Intelligent Robots and Systems (IROS), Hamburg, Germany, 2015: 1552-1557

[20] Kazama E, Sato R, Miyamoto I, et al. Development of a small quadruped robot with bi-articular muscle-tendon complex[C]//Proceedings of the 2015 IEEE International Conference on Robotics and Biomimetics (ROBIO), Zhuhai, China, 2015: 1059-1064

Chen Ziheng, born in 1994. He received his B. S. degree from Shandong University of Technology in 2017. Now he is a master student in School of Mechatronic and Engineering Automation, Shanghai University. His research interest is bionic robot technology.